Large Eddy Simulation of the Effect of Hull on Marine Propulsors in Crashback

Aman Verma, Hyunchul Jang, Krishnan Mahesh

Aerospace Engineering and Mechanics, University of Minnesota, Minneapolis, USA

ABSTRACT

Presence of the hull significantly increases the side-forces on a propulsor in crashback below J=-0.7 (Bridges, 2004). Large Eddy Simulation (LES) reproduces the experimentally observed behavior. LES is performed for an open propulsor with and without hull at two advance ratios, J=-1.0 and J=-0.5. At J=-1.0, two noticeable flow features are found with the hull - a recirculation zone upstream in the vicinity of the propulsor and a ring vortex much closer to the propulsor. In contrast, at J=-0.5, there is a much smaller recirculation zone which is further upstream due to the increased reversed flow. As a result, the hull does not make much difference in the immediate vicinity of the propulsor at J=-0.5. For both advance ratios, side forces are mostly generated from the leading edge separation on suction side. However, high levels of side forces are also generated from trailing edge separation on suction side at J=-1.0. The trailing edge separation is related to the upstream recirculation zone.

Keywords

Large eddy simulation, propulsors, crashback, hull.

1 INTRODUCTION

Crashback is an operating condition where the propulsor rotates in the reverse direction while the vessel moves in the forward direction. Since the crashback condition is dominated by large scale unsteadiness, it is well known as one of the most challenging to analyze. Low frequency components of the unsteadiness can affect propulsor thrust, torque, and side-force, which affect maneuverability of the vessel during crashback condition.

The crashback condition is dominated by the interaction of the free stream flow with the strong reversed flow from propulsor rotation as shown in figure 1. This interaction forms the unsteady ring vortex that is the most remarkable aspect of the flow during crashback operation.

Jiang et al. (1996) studied the structure of the unsteady vortex ring using Particle Image Velocimetry (PIV) measurements. They noted that the unsteady vortex ring is related to unsteady shaft forces and the oscillation frequency of the ring vortex is much lower than the propulsor rotation rate. Jessup et al. (2004) presented more detailed measurements of flow velocity fields using PIV and Laser Doppler Velocimetry (LDV).

The computational prediction of the flow around marine propulsors has been performed using unsteady Reynolds-Averaged Navier-Stokes equations (RANS) (Chen & Stern, 1999; Davoudzadeh et al., 1997). They showed that RANS yielded good results for forward and backing modes, but produced significant discrepancies in crashback and crashahead modes.

The cross-section of a propulsor blade with the cylindrical surface resembles an airfoil. Under the crashback condition, the leading and trailing edges of propulsor blades exchange their roles. The sharp trailing edge of normal conditions becomes the leading edge so that large flow separations could occur at the sharp leading edge. The large flow separations may cause high amplitude fluctuation of unsteady loads. Large Eddy Simulation (LES) is therefore an attractive computational methodology for predicting the fluctuating forces. Since RANS is based on time average or ensemble average, it cannot accurately predict high fluctuation of unsteady loads.

Mahesh et al. (2004) developed a non-dissipative and robust finite volume method with LES on unstructured grids. Vyšohlíd & Mahesh (2006) performed numerical simulations of crachback condition with the code at the advance ratio J=-0.7. They showed that LES could yield good agreement for mean and rms values of unsteady loads. The computed power spectral density for unsteady loads showed the same peak as the experiment at 5 rev[-1]. Jang & Mahesh (2010) introduced two quantities for pressure contributions to thrust and side-force to give a clearer understanding about the origin of thrust and side-force. They also used conditional averaging to study the flow field. Chang et al. (2008) performed LES at other advance ratios, J=-0.5 and J=-1.0 with the same LES code and computational grid as Vyšohlíd & Mahesh (2006). They investigated instantaneous flow fields at a high thrust event and a low thrust event to understand the
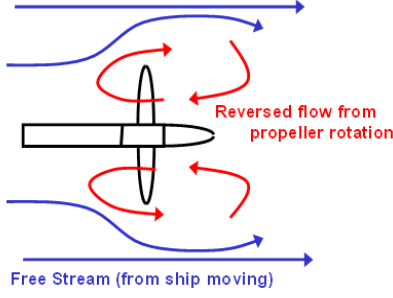
Figure 1. Schematic of crashback condition.

physics of crashback. They reported that a bi-modal behavior with vortex ring and axial jet modes occurred at low negative J. At high negative J, the flow only acted in ring vortex mode.

In the present work, flow past the propulsor blades with an upstream submarine hull is considered. ONR-body 1 is used for the hull geometry. Now the inflow to the propulsor blades is not the freestream but the wake of the hull. Bridges' experiment (Bridges' 2004) noted that the side-forces increased dramatically below an advance ratio of J=-0.7 when the hull is present (figure 2). However the reason for this discrepancy is not well understood. The objectives of the present work are to: (1) evaluate the ability of LES to predict this hull effect and (2) provide a physical explanation.

2 SIMULATION DETAILS

2.1 Numerical Method

Simulations are performed in a frame of reference that rotates with the propulsor. The incompressible Navier-Stokes equations in the rotating frame of reference can be formulated in a strongly conservative form (Beddhu et. al., 1996) or in a form where system rotation produces a source term (Majety, 2003). Also, the governing equations can either be written for the absolute velocity vectors in the stationary frame or for the relative velocity vectors in rotating frame. Here, the rotational source term is chosen with the absolute velocity.

In LES, large unsteady motions are directly solved with spatially filtered equations, whereas effects of small scale motions are modeled. The spatially filtered momentum equation in the rotating frame of reference is

$$\frac{\partial \overline{u_i}}{\partial t} + \frac{\partial}{\partial x_j}\left(\overline{u_i u_j} - \overline{u_i}\varepsilon_{jkl}\omega_k x_l\right) =$$
$$-\frac{\partial \overline{p}}{\partial x_i} - \varepsilon_{ijk}\omega_j\overline{u_k} + \nu\frac{\partial^2 \overline{u_i}}{\partial x_j \partial x_j} - \frac{\partial \tau_{ij}}{\partial x_j} \quad (1)$$

$$\frac{\partial \overline{u_i}}{\partial x_i} = 0$$

with the approximation $\overline{u_i\varepsilon_{jkl}\omega_k x_l} \approx \overline{u_i}\varepsilon_{jkl}\omega_k x_l$.

u_i are the inertial velocities in the stationary frame, p is the pressure, x_i are coordinates in the rotating non-inertial reference frame, ω_j is the angular velocity of the rotating frame of reference, ν is the kinematic viscosity, ε_{ijk} denotes the permutation symbol for the tensor
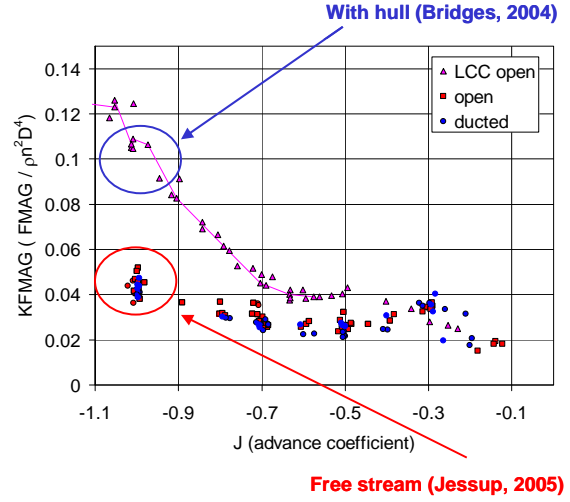

Figure 2. Increase in side-force magnitude with hull below J=-0.7. (Jessup, 2006)

notation, $\overline{}$ denotes the spatial filter, $\tau_{ij} = \overline{u_i u_j} - \overline{u_i}\,\overline{u_j}$ is the sub-grid stress. The sub-grid stress is modeled by the dynamic Smagorinsky model (Germano et al., 1991; Lilly, 1992).

Eq. (1) is solved by a numerical method developed by Mahesh et al. (2004) for incompressible flows on unstructured grids. The algorithm is derived to be robust without numerical dissipation. It is a finite volume approach which stores the Cartesian velocities and the pressure at the centroids of the cells and the face normal velocities are stored independently at the centroids of the faces. A predictor-corrector approach is used. The predicted velocities at the control volume centroids are first obtained and then interpolated to obtain the face normal velocities. The predicted face normal velocity is projected so that continuity is discretely satisfied. This yields a Poisson equation for pressure which is solved iteratively using a multigrid approach. The pressure field is used to update the Cartesian control volume velocities using a least-squared formulation. Time advancement is performed using an implicit Crank-Nicholson scheme. The algorithm has been validated for a variety of problems (Mahesh et al., 2004) over a range of Reynolds numbers.

2.2 Propulsor Geometry, Computational Mesh and Boundary Conditions

Simulations are performed for a marine propulsor P4381, which is a five-bladed, right-handed with variable pitch, no skew and rake. The propulsor has been used in various experiments (Jiang et al., 1997; Jessup et al., 2004; Jessup et al., 2006) and computations (Davoudzadeh et al., 1997; Chen & Stern, 1999; Vyšohlíd & Mahesh, 2006; Chang et al., 2008; Jang & Mahesh, 2010). The detailed propulsor geometry and hub geometry are given in Jessup et al. (2006).

The computational domain is a cylinder with the diameter of 7.0D and the length of 14.0D where D is the diameter of the propulsor disk. Half body of the hull is used and stabilizing fins are ignored. Free-stream
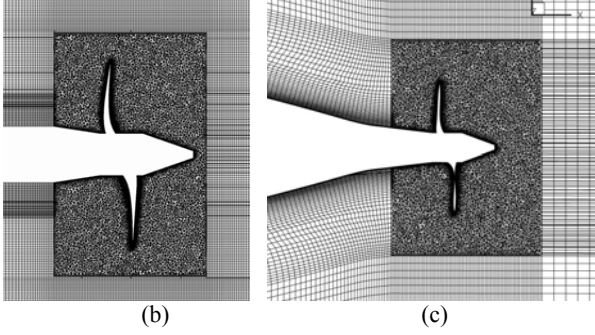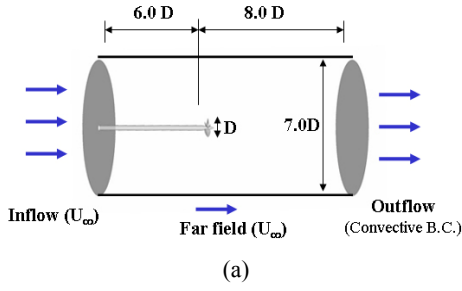
Figure 3. (a) Computational domain and boundary conditions on domain boundaries; Computational grids: (b) XY plane of grid for propulsor without hull, (c) XY plane of grid for propulsor with hull.

velocity boundary conditions are specified at the inlet and the lateral boundaries. Convective boundary conditions are prescribed at the exit. As mentioned, boundary conditions on solid walls are forced as those are prescribed in the inertial reference frame. Thus, boundary conditions on rotor part, blades and hub, are specified as $u = \omega \times r$, while those on that hull or shaft are prescribed as no-slip boundary conditions. The computational domain, boundary conditions and XY planes of the grids are shown in figure 3.

In the LES of propulsor without hull at J=-0.7 by Jang & Mahesh (2010), the number of elements is 19.3 million. In the present work, simulations are performed for the propulsor with and without hull at J=-1.0 and J=-0.5. The propulsor without hull has 7.7 million elements and the propulsor with hull 7.3 million elements.

3 RESULTS

Large-Eddy Simulations were performed under the crashback condition at negative advance ratios and Reynolds number Re = 480,000. The advance ratio J and Reynolds number Re are defined as

$$J = \frac{U}{nD}, \quad \mathrm{Re} = \frac{DU}{\nu} \qquad (2)$$

where U is the free-stream velocity, n is the propulsor rotational speed, and D is the diameter of the propulsor disk. According to Jessup et al. (2004)'s experiments, thrust and torque do not depend on Reynolds number where $4 \times 10^5 < \mathrm{Re} < 9 \times 10^5$. The Reynolds number Re=480,000 is within this range.

Thrust T is the axial component of force. Torque Q is the

axial component of the moment of force. F_H and F_V are the horizontal and vertical projections of the force. Their vector sum is the projection of the force onto the direction perpendicular to the propulsor axis and is termed the side-force S. Since computations are performed in the rotating frame of reference, the side-force is translated to the inertial reference frame. The horizontal and vertical components of the side-force, F_H and F_V, respectively, can be obtained from a rotational transformation using the angle between the rotating frame and the inertial frame.

Non-dimensional thrust coefficient K_T, torque coefficient K_Q and side-force coefficient K_S are given by

$$K_T = \frac{T}{\rho n^2 D^4}, \quad K_Q = \frac{Q}{\rho n^2 D^5}$$

$$K_S = \frac{\sqrt{F_H^2 + F_V^2}}{\rho n^2 D^4} \qquad (3)$$

where ρ is the density of the fluid.

3.1 Propulsor without hull at J=-0.7

The LES of propulsor without hull at J=-0.7 by Jang & Mahesh (2010) is in good agreement with the experimental results of Jessup et. al. (2004, 2006). WT denotes 36″-water tunnel experiment and OW is towing-tank experiment. As shown in table 1, computed mean K_T and K_Q are located between water tunnel and towing-tank results.

	$<K_T>$	$<K_Q>$	$<K_S>$
LES (2010)	-0.37	-0.074	0.023
WT (2004)	-0.33	-0.065	0.024
OW (2006)	-0.41	-0.078	-

Table 1. J=-0.7: Mean values of thrust, torque and side-force magnitude given by previous computation and experiments.

Figure 4 shows that the circumferentially averaged flow fields computed by them also compare favorably with those measured with LDV by Jessup et al. (2004). Table 2 shows reasonable agreement between computed and experimental locations of the center of the vortex ring.

3.2 Effect of Hull at J=-1.0

The time history of K_S is shown in figure 5(a), (b). $< \cdot >$ denotes the mean value and $(\cdot)'$ denotes standard deviation. The time history is shown over 181 propulsor rotations for propulsor without hull and 204 for propulsor with hull. The horizontal lines in figure 5 are the mean and the mean plus or minus standard deviation. Since K_S is positive, $<K_S>-(K_S)'$ represents low side-force and $<K_S>+(K_S)'$ means high side-force. As shown in Table 3 computed side-force magnitude shows good agreement with the experimental results for propulsor with and without hull at J=-1.0. The LES predicts the experimentally observed increase in side-force in the presence of the hull.

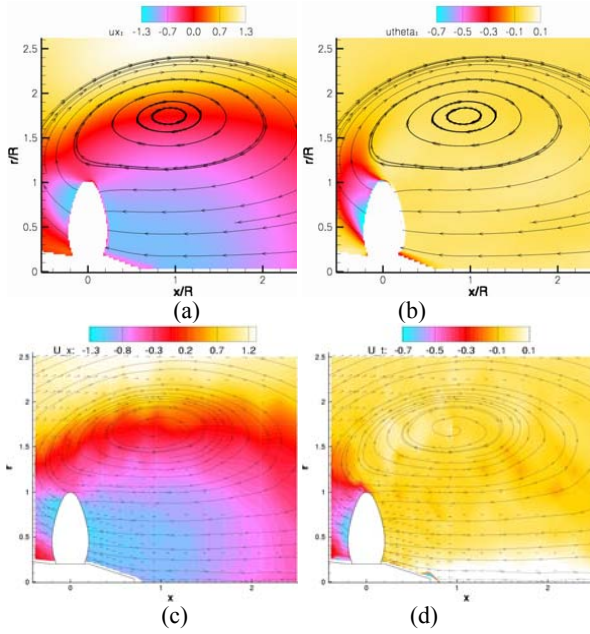Figure 4. J=-0.7: Circumferentially averaged flow fields. (a) axial velocity and (b) tangential velocity (LES; Jang & Mahesh, 2010), (c) axial velocity and (d) tangential velocity (experiment; Jessup et al., 2004)

	x_cen / R	r_cen / R
LES (2010)	0.93	1.75
WT (2006)	0.96	1.71

Table 2. J=-0.7: Location of center of vortex ring obtained from circumferentially averaged flow fields from computation and experiment.

3.2.1 Time averaged flow field

Time averaged statistics of flow field are computed over 172 propulsor rotations for propulsor without hull and 170 rotations with hull which is within the time window for which the time history of K_S is shown. Figure 6 shows an XY plane slice cutting the center and along the length of the shaft/hull. Time averaged pressure and velocity streamlines are plotted. Flow features distinguishing the presence of the hull are clearly observed.

The velocity streamlines in figure 6 reveal a recirculation zone upstream of the blades in the presence of the hull. No such recirculation zone appears near the shaft without hull. This region of high circulation is created by the interaction between the wake of the hull and reversed flow produced by propulsor rotation. Also, the center of vortex ring is observed closer to blades with hull. The suction side of the blades with hull see lower levels of pressure than without hull. Reverse rotation also causes reversed flow without the hull, but the flow interacts with a freestream which enters the propulsor disk with higher momentum than the hull wake.

3.2.2 Circumferentially averaged flow field

The time averaged flow statistics are further averaged along lines of constant radius to yield circumferentially averaged statistics in the X-R plane. Figure 7 shows
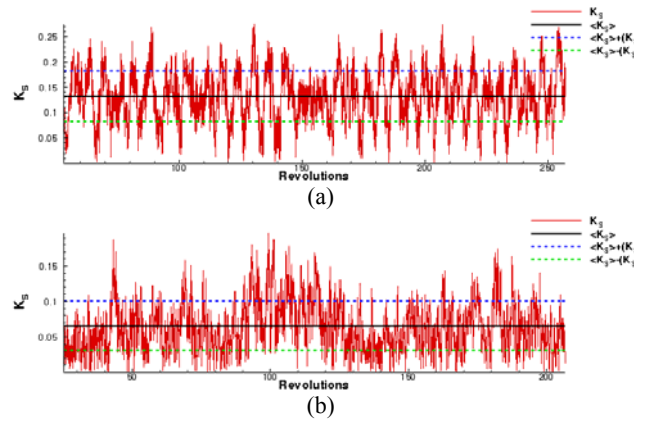

Figure 5. J=-1.0: Time history of unsteady loads on the blades. Side-force coefficient K_S (a) w/ hull, (b) w/o hull.

|		$<K_S>$	$(K_S)'$
Hull	LES	0.132	0.049
	Experiment (Bridges, 2004)	0.105 ~0.126	-
Without hull	LES	0.064	0.034
	Experiment (Jessup, 2005)	0.036 ~0.052	0.022

Table 3. J=-1.0: Computed and experimental values of mean and rms of magnitude of side-force on the blades with and without hull.

contours of axial velocity with streamlines with and without hull. The blanked out zone is where the hull/shaft and the propulsor blade would be. The upstream recirculation zone is nestled between the blades and the rising contours of the hull centered at the coordinates (x/R, r/R) ≡ (-1.03, 0.51). Note that the vortex ring is much closer to the tip of the blade when the hull is present. The upstream recirculation region reduces the streamwise momentum of upstream flow which causes the ring vortex to be created closer to the blade with hull. Table 4 compares the locations of the center of the vortex ring with and without hull.

Velocity profiles are extracted from three x-locations upstream of the blade. One of these locations (x/R=-1.0) passes close to the center of the recirculation region in the simulation with hull (x/R=-1.03) and the velocity profile at this location is shown in figure 8(a). The black solid line is for the propulsor with hull while the dotted red line is without hull. Figure 8(a) shows the difference that the presence of a hull makes. The velocity profile with hull in figure 8(a) clearly indicates a low momentum velocity profile compared to without hull. In fact, there is even slightly reversed velocity close to the hull body (r/R<0.5). Not surprisingly, this is close to the center of the recirculation zone. In figures 8(b) and 8(c), lower velocity with hull is observed for r/R>1.4. This can explain our assertion that lower momentum of the incoming upstream flow causes the center of the vortex ring to be located closer to the blades with hull.
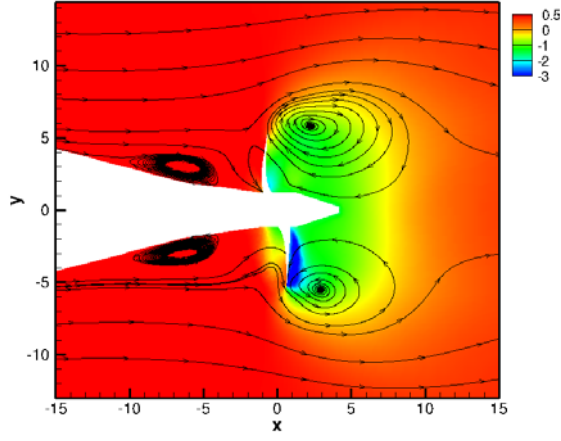
(a)
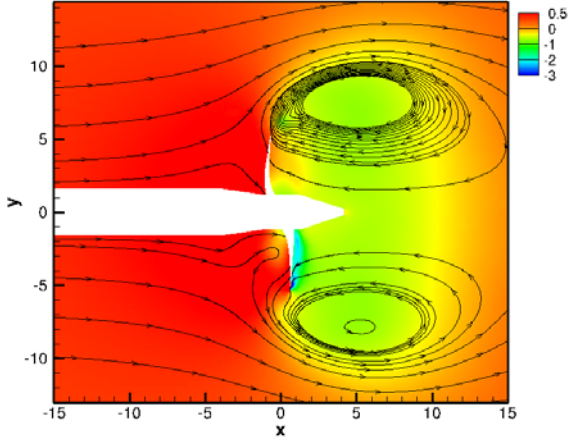
(b)

Figure 6. J=-1.0: Time averaged pressure contours with streamlines (a) w/ hull (b) w/o hull.

3.3 Higher side-force with hull

During crashback, the leading and trailing edges reverse roles. Hence, what would usually be the leading edge during normal mode of operation would become the trailing edge during the crashback maneuver and vice-versa. The leading (LE) and trailing edges (TE) of the propulsor blades are defined as follows. LE is the downstream edge of the blade which first sees the reversed flow due to propulsor rotation and TE is the other end.

At high Reynolds numbers, viscous effects are smaller in comparison to pressure effects. Hence pressure force is the dominant term in blade loadings. Jang & Mahesh (2010) introduced two quantities for pressure contributions to thrust and side-force given as
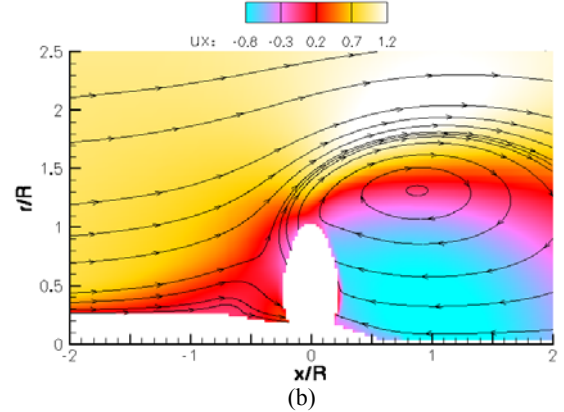
$$(\text{Thrust}) = \vec{F} \cdot \vec{i} = \sum_{f=\text{faces}} p\,(\vec{n}_f \cdot \vec{i}) A_f \tag{4}$$

$$(\text{Side force}) = \sqrt{(\vec{F} \cdot \vec{j})^2 + (\vec{F} \cdot \vec{k})^2}$$
$$= \sum_{f=\text{faces}} |p| \sqrt{(\vec{n}_f \cdot \vec{j})^2 + (\vec{n}_f \cdot \vec{k})^2}\, A_f \tag{5}$$

where p is the pressure, $\vec{n}_f$ is the outward normal vector of the face, A_f is the area of the face and the force vector $\vec{F}$ is summed up over all faces f on the propulsor surface.
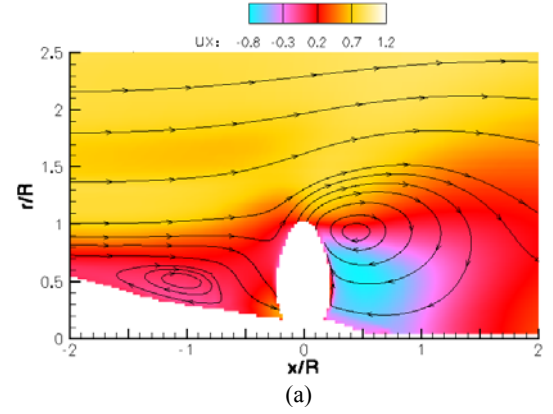
(a)

(b)

Figure 7. J=-1.0: Circumferentially averaged axial velocity with streamlines (a) w/ hull (b) w/o hull.

	x_cen / R	r_cen / R
Hull	0.45	0.94
Without hull	0.88	1.32

Table 4. J=-1.0: Locations of centers of vortex rings with and without hull from circumferentially averaged flow fields.

(a)   (b)   (c)

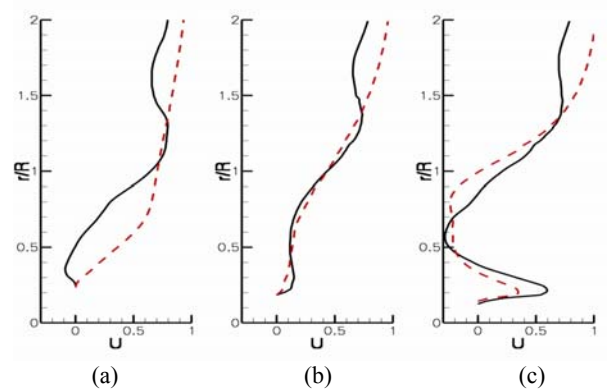**Figure 8. J=-1.0: Axial velocity profiles from 3 x-locations upstream of the blades; —— w/ hull; ─ ─ w/o hull; (a) x/R=-1.0, (b) x/R=-0.5, (c) x/R=-0.2.**

In order to understand the mechanism of generation of higher side-forces at J=-1.0 when a hull is present, two quantities are examined: (1) rms of effective pressure for side-force magnitude on the propulsor blades and (2) mean pressure around the blades near the blade root.

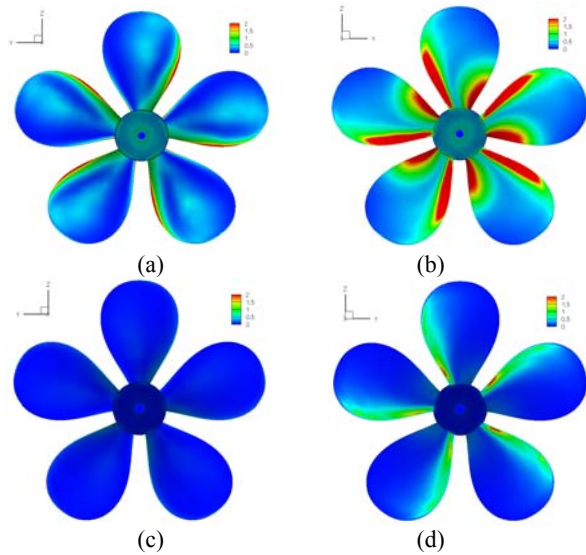The side of the propulsor blade facing the incoming hull

Figure 9. J=-1.0: RMS of effective pressure contribution to side-force on (a) pressure side (b) suction side (w/ hull) (c) pressure side (d) suction side (w/o hull).

wake or freestream is the pressure side and the other side towards the reversed flow is the suction side. Figures 9(a)-(d) show that the rms of effective pressure for side-force magnitude is significantly higher with hull. Even on the pressure side, propulsor with hull (figure 9(a)) has higher level of rms effective pressure than without hull (figure 9(c)). This is especially true for the suction side as shown in figure 9(b). Just considering the suction side for propulsor with hull (figure 9(b)), most of the contribution comes from LE as compared to the TE. Comparing figures 9 (b) and (d), even the TE on the suction side with hull shows a higher pressure contribution to side-force. This observation for propulsor without hull is in keeping with that by Jang & Mahesh (2010) at J=-0.7.

Closer inspection of the TE reveals that most of the pressure contribution towards high side-force magnitude comes from near the blade root. Figure 10 shows time averaged pressure contours in cross-planes near the blade root at a constant radius of r/R=0.4. From figure 10(a), the LE for propulsor with hull shows lower pressure than without hull. This could point towards higher separation at LE with hull. The TE for propulsor with hull also sees lower pressure than without hull and could be a region for a small separation region.

3.4 Mechanism of higher side-force with hull
The schematic in figure 11 attempts to explain the existence and formation of the separation zones near the LE and TE of the blades with hull.

As has been established earlier (in section 3.2.2), the propulsor blades with hull see a larger inward motion towards them due to greater reversed flow. Also, the vortex ring is located closer to the blades. Therefore, the LE sees larger incoming flow at a higher angle of attack. This leads to larger LE separation with hull.

From figure 8, it is observed that the velocity near the blade root with hull is greater than without the hull. This
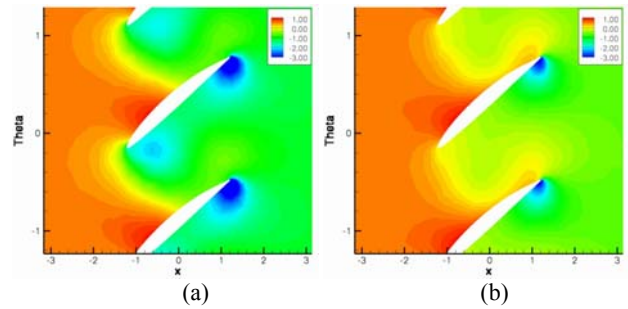

Figure 10. J=-1.0: Time averaged pressure field in cross-planes at constant radius r/R=0.4: (a) w/ hull (b) w/o hull.
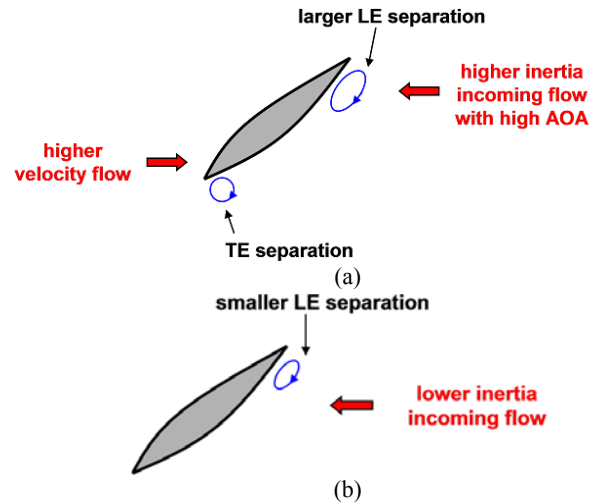

Figure 11. J=-1.0: Explanation for formation of separation zones on blades near blade root for propulsor (a) w/ hull (b) w/o hull.

would imply a larger incoming flow towards the TE of the blade near the blade root, resulting in a greater TE separation zone with hull. This could explain the lower pressure regions near the LE and TE of the blades with hull as shown in figure 10.

To summarize, propulsor with hull has lower mean pressure and possibly greater separation at the LE and TE on the suction side. It also has much higher levels of rms of effective pressure for side-force magnitude on the LE and TE of the suction side. The striking difference with propulsor without hull is that even the TE contributes to higher side-forces.

3.5 Effect of hull at J=-0.5
Simulations are performed for the propulsor with and without hull at J=-0.5. J=-0.5 is chosen because it is higher than the critical advance ratio of J=-0.7 mentioned by Bridges (2004). According to the experiments, the presence of an upstream hull is not expected to make much of a difference to the performance of the propulsor in crashback.

Table 5 shows that the hull does not change the mean and rms of the side-force magnitude by much at J=-0.5 These values are computed over 140 propulsor rotations for propulsor without hull and 200 rotations for propulsor with the hull. The time averaged statistics shown in figure 12 are, though, computed over 153 rotations for propulsor with the hull.
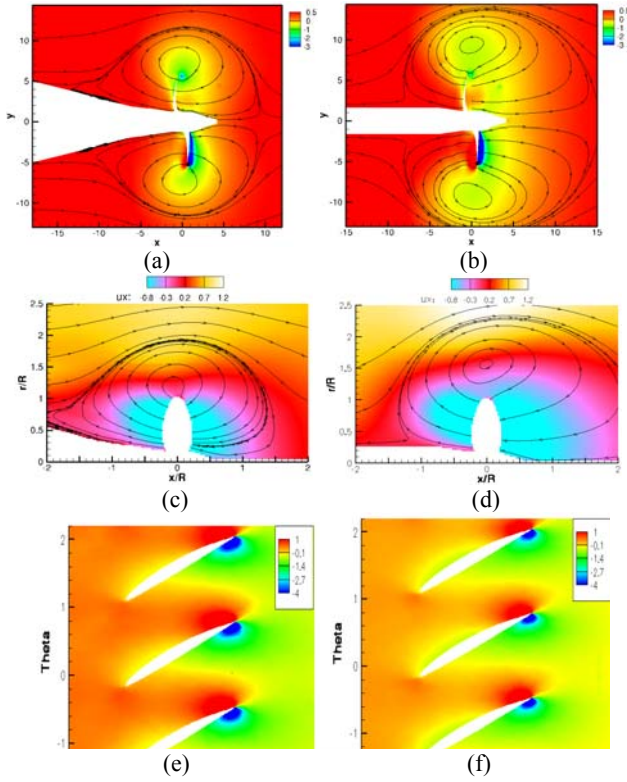
(a)   (b)

(c)   (d)

(e)   (f)

Figure 12. J=-0.5: Time averaged pressure contours with streamlines: (a) w/ hull (b) w/o hull; Circumferentially averaged axial velocity with streamlines: (c) w/ hull (d) w/o hull Time averaged pressure field in cross-planes at constant radius r/R=0.4: (e) w/ hull (f) w/o hull.

Figures 12(a), (b) show the time averaged pressure contours with streamlines. Note that compared to figure 6(a) earlier for J=-1.0, there is a much smaller recirculation zone and it is located further upstream of the blades now. The ring vortex is also located closer to the blades and figure 12(c) shows that there is only a slight radially inward displacement in the location of the center of the ring vortex with hull. Importantly, it is observed that the propulsor blades see a higher velocity inflow from the reversed flow compared to that at J=-1.0.

Figure 13(a) shows the axial velocity profiles for both with (solid black) and without hull (dotted red) at J=-0.5. The profile is taken at an x-location (x/R=-2.0) upstream on the hull/shaft which passes through the small recirculation zone when the hull is present. Note the similarity of this profile to figure 8(a) which was also taken at an x-location which passed through the center of the recirculation zone for J=-1.0. Figure 13(b) shows axial velocity profiles in the near-field of the propulsor blades (x/R=-0.2). The velocity profile for propulsor with hull at J=-1.0 (dash-dotted blue here; solid black in figure 8(c)) is also plotted alongwith those with and without hull at J=-0.5. Note that in the near-field of the blades, the hull does not make much of a difference till the blade radius (r/R<1) at J=-0.5 and the axial velocities are much more negative than what the hull saw at J=-1.0. This increased reversed flow extends from about a radius downstream of the blades to about a radius upstream.
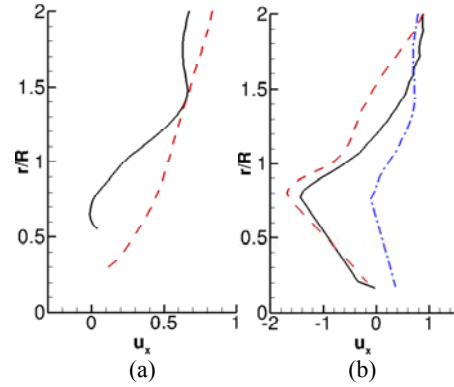

(a)   (b)

Figure 13. Axial velocity profiles from x-locations upstream of the blades; J=-0.5: —— w/ hull, – – – w/o hull; J=-1.0: – · – w/ hull; (a) x/R=-2.0, (b) x/R=-0.2.

	$\langle K_S \rangle$	$(K_S)'$
Hull	0.023	0.013
Without hull	0.022	0.012

Table 5. J=-0.5: Computed values of mean and rms of magnitude of side-force on the blades with and without hull. For experimental values, refer to figure 1.

Comparing it to figure 7(a) earlier, this was not the case at J=-1.0 where immediately upstream of the blades, the wake of the hull interacts with the reversed flow to produce the recirculation zone. Also, looking at figure 7(b), it can be said that even without the influence of the hull, the reversed flow is not strong enough to extend upstream beyond the blades.

3.6 Mechanism of different side-force at different advance ratios

The above results suggest the following model to explain the mechanism of different side-force magnitudes at different advance ratios. At lower negative advance ratio, such as J=-0.5 (figure 14(b)), the rotational rate of the propulsor blades is high enough to cause a higher reversed flow into the blades. This reversed flow interacts with the hull at a greater upstream distance from the propulsor, thus suppressing the formation of a recirculation zone. Velocities upstream of the blades are still high enough and so the ring vortex is formed further off the blades. As a result, the hull does not make much of a difference to the flow when the propulsor rotation rate is higher which is same as a lower negative advance ratio. Hence results with and without hull are similar at J=-0.5.

As has been explained earlier in section 3.4, a closer ring vortex and recirculation zone leads to greater separation on the LE and TE respectively on the suction side of the blade. At J=-0.5, the vortex ring is relatively close to the blades and this causes separation on the LE of the suction side leading to the low pressure region seen in figure 12(e), (f). But there is no corresponding low pressure region on the TE and this could be attributed to the absence of the recirculation region. Figure 15 shows that at J=-0.5, the side-force for both with and without hull arises from the LE on the suction side.
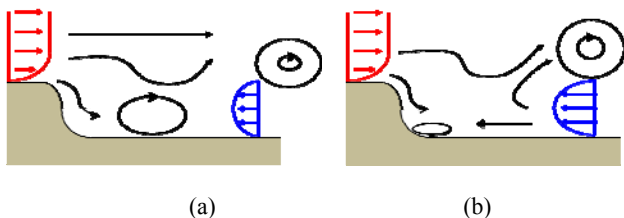
(a)   (b)

Figure 14. Schematic to explain flow in the presence of a hull at (a) high negative advance ratio (J=-1.0) (b) low negative advance ratio (J=-0.5).

(a)   (b)

Figure 15. J=-0.5: rms of effective pressure contribution to side-force on suction side (a) w/ hull (b) w/o hull.

4 CONCLUSION

Crashback simulations for an open propulsor with and without hull have been performed at the advance ratios J=-0.5 and J=-1.0. According to Bridges' experiment with the upstream hull, side forces increase dramatically as J is reduced below -0.7. At J=-1.0, computed mean and rms of the coefficient of side-force magnitude show good agreement with the experimental data for both with and without hull. Two new noticeable flow features are found with the hull at J=-1.0. A recirculation zone is found to exist upstream of the propulsor blades and the center of the ring vortex is located much closer to the propulsor blades. The presence of the hull decreases the momentum of the flow which causes the ring vortex to be located closer to the blades. At low negative J (J=-0.5), the upstream recirculation zone is suppressed because the reversed flow from propulsor rotation is higher. The effective pressure for side force with hull is significantly higher than without hull. For both advance ratios, the side force with hull is mostly generated from leading edge separation on suction side. However, higher magnitude of side-forces are also generated from trailing edge separation on suction side at J=-1.0. Higher separation on both the leading and trailing edges of the suction side of the blade cause higher side-forces in the presence of a hull at J=-1.0

REFERENCES

Beddhu, M., Taylor, L. K., Whitfield, D. L. (1996), 'Strong Conservative Form of the Incompressible Navier-Stokes Equations in a Rotating Frame with a Solution Procedure', Journal of Computational Physics, Vol. 128, pp. 427-437.

Bridges, D.H., (2004), 'A detailed Study of the Flowfield of a Submarine Propeller During a Crashback Maneuver', Aerospace Engineering, Mississippi State University, Report No. MSSU-ASE-04-1.

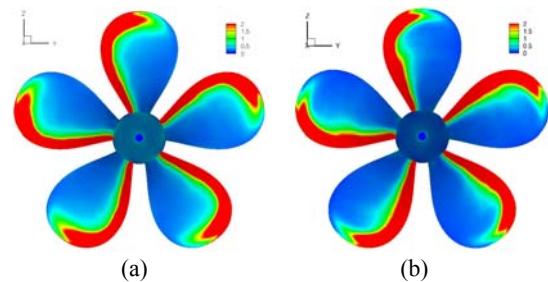Chang, P., Mahesh, K. (2006), 'Large Eddy Simulation of Crashback in Marine Propulsors', Proceedings of the 26th Symposium on Naval Hydrodynamics, Rome.

Chen, B., Stern, F. (1999), 'Computational Fluid Dynamics of Four Quadrant Marine Propulsor Flow', Journal of Ship Research, Vol. 43, No. 4, pp. 218-228.

Davoudzadeh, F., Taylor, L. K., Zierke, W. C., Dreyer, J. J., McDonald, H., Whitfield. D. L. (1997), 'Coupled Navier-Stokes and Equations of Motion Simulation of Submarine Maneuvers, Including Crashback', Proceedings of the 1997 ASME Fluids Engineering Division Summer Meeting, Vol. 2, New York.

Germano, M., Piomelli, U., Moin, P., Cabot, W. H. (1991), 'A dynamic Subgrid-Scale Eddy Viscosity Model', Physics of Fluids A, Vol. 3, No. 7, pp.

Jang, H., Mahesh K. (2010), 'Large Eddy Simulation of Marine Propulsors in Crashback', 28st Symposium on Naval Hydrodynamics, Pasadena, California.

Jiang, C. W., Dong, R. R., Lui, H. L., Chang, M. S. (1997), '24-inch Water Tunnel Flow Field Measurements During Propulsor Crashback', 21st Symposium on Naval Hydrodynamics, The National Academies Press, Washington DC, pp. 136-146.

Jessup, S., Chesnakas, C., Fry, D., Donnelly, M., Black, S., Park, J. (2004), 'Propulsor Performance at Extreme Off Design Conditions', Proceedings of the 25th Symposium on Naval Hydrodynamics, Canada.

Jessup, S., Fry, D., Donnelly, M. (2006), 'Unsteady Propulsor Performance in Crashback Conditions With and Without Duct', Proceedings of the 26th Symposium on Naval Hydrodynamics, Rome, Italy.

Lilly, D. K. (1992), 'A Proposed Modification of the Germano Subgrid-Scale Closure Model', Physics of Fluids A, Vol. 4, No. 3, pp. 633-635.

Majety, K., S. (2003), 'Solutions to the Navier-Stokes Equations in Non-Inertial Reference Frame', PhD thesis, Mississippi State University.

Mahesh, K., Constantinescu, G., Moin, P. (2004), 'A Numerical Methods for Large-Eddy Simulation in Complex Geometries', Journal of Computational Physics, Vol. 197, No. 1, pp. 215-240.

Vyšohlíd, M., Mahesh, K. (2006), 'Large Eddy Simulation of Crashback in Marine Propulsors', Proceedings of the 26th Symposium on Naval Hydrodynamics, Rome.